ARTICLE IN PRESS
TECTO-124876; No of Pages 14

Tectonophysics xxx (2010) xxx–xxx

Contents lists available at ScienceDirect

Tectonophysics

journal homepage: www.elsevier.com/locate/tecto

Static Coulomb stress changes on faults caused by the 2008 Mw 7.9 Wenchuan, China earthquake

Yongge Wan [a,*], Zheng-Kang Shen [b,c]

[a] Institute of Disaster Prevention Science and Technology, Yanjiao, Sanhe City, Hebei Province 065201, China
[b] Department of Geophysics, School of Earth and Space Science, Peking University, Beijing 100871, China
[c] Department of Earth and Space Sciences, UCLA, Los Angeles, CA 90095-1567, USA

ARTICLE INFO

Article history:
Received 18 February 2009
Received in revised form 4 February 2010
Accepted 24 March 2010
Available online xxxx

Keywords:
The Wenchuan earthquake
Coulomb failure stress change
Fault interactions
Seismic hazard potential

ABSTRACT

The 12 May 2008 Mw 7.9 Wenchuan earthquake has changed the regional tectonic stress field significantly. It is important to know how such a change affects the tectonic loading processes of the faults and therefore the seismic potential of the region. Utilizing the slip distribution of the Wenchuan earthquake as the driving source we compute the changes of Coulomb failure stress (*CFS*) on the neighborhood faults assuming a friction coefficient of 0.4. Our results show that the *CFS*s have increased on average 1.6×10^4 and 1.8×10^4 Pa at the SW and NE ends of the Longmen Shan, 2.6×10^4 Pa at the western segment of the Qinling Southern Frontal, 2.0×10^4 Pa at the northernmost part of the Longriba, 1.4×10^4 Pa at the southernmost part of the Xianshuihe, 1.3×10^4 Pa at the southeast end of the East Kunlun, 9.0×10^3 Pa at the southernmost part of the Minjiang, 2.9×10^3 Pa at the Baiyu, and 3.5×10^3 Pa at the Longxian–Baoji faults. Recurring times of these faults are advanced, about 39 and 230 years for the SW and NE segments of the Longmen Shan, ~5.5 years toward the east end of the East Kunlun, and ~1.6 years for the SE segments of the Xianshuihe faults. The quake also relaxed the *CFS* significantly on most part of the Minjiang, southwest segment of the Longriba, northwest segment of the Xianshuihe, southeast segment of the Yushu–Maqu, north part of the Xiaojinhe, Daliangshan, and Anninghe faults, with the *CFS* reductions ranging on average of 1.8×10^4, 2.5×10^4, 7.1×10^3, 2.4×10^3, 1.0×10^3, 1.0×10^3, and 1.6×10^3 Pa, respectively. Recurring times of these faults are delayed, up to 185 years for the south segment of the Minjiang, up to 18 years for the northeast of the Longriba, up to 9.8 years for the West Qinling Northern Frontal, and up to 2.7 years for the northwest segment of the Xianshuihe faults, respectively. We test sensitivity of the changes of *CFS* to variations of apparent fiction coefficient μ', and find that the senses of *CFS* change are almost invariant with μ' except at the Minjiang, Longriba, and Qinling Southern Frontal faults, where large normal stresses on faults induced by the Wenchuan earthquake could play an important role in manifesting *CFS* change when μ' is large. The *CFS* changes vary slowly along seismogenic depth on most of the receiver faults.

1. Introduction

On May 12, 2008, an Mw 7.9 earthquake struck Wenchuan county, Sichuan province in south China (Fig. 1). This quake ruptured the central section of the Longmen Shan fault located between the eastern rim of the Tibetan plateau to its northwest and the Sichuan basin to its southeast. Occurrence of the quake is part of a tectonic process in which a slowly eastward moving Tibetan plateau collides with a mechanically strong Sichuan basin. The eastern rim of the Tibetan plateau bordering the Sichuan basin is known to have had destructive earthquakes in the past century. For example, an M7.3 event occurred at Diexi in August 1933 (Kan et al., 1977) and a M7.2 doublet event occurred at Songpan in August 1976 (Molnar and Deng, 1984), both located only about 100 km northwest of the Longmen Shan fault system (Fig. 1).

The Longmen Shan range is a prominent boundary between the eastern Tibetan plateau and the Sichuan basin. The flat basin is in remarkable contrast with the Longmen Shan range whose average elevation rises up for about 3 km within about 100 km distance into the plateau (Burchfiel et al., 1995). High P wave velocity is found in the lower crust and upper mantle down to about 250 km depth beneath the Sichuan basin, enabling the craton-like basin to resist deformation in the Mesozoic and Cenozoic time (Burchfiel et al., 1995; Wang et al., 2003). The crust underneath the Longmen Shan range and the eastern Tibetan plateau, on the other hand, is believed to be much weaker mechanically, with low seismic velocity zones widely developed in the lower crust (Wang et al., 2003; Yao et al., 2008). The Longmen Shan fault system,

* Corresponding author. Department of Earthquake Science, Institute of Disaster Prevention Science and Technology, Yanjiao, Sanhe City, Hebei Province, 065201, China. Tel.: +86 10 61597607.
E-mail addresses: wanyg217217@vip.sina.com.cn (Y. Wan), zhengkangshen@pku.edu.cn (Z.-K. Shen).

0040-1951/$ – see front matter © 2010 Elsevier B.V. All rights reserved.
doi:10.1016/j.tecto.2010.03.017

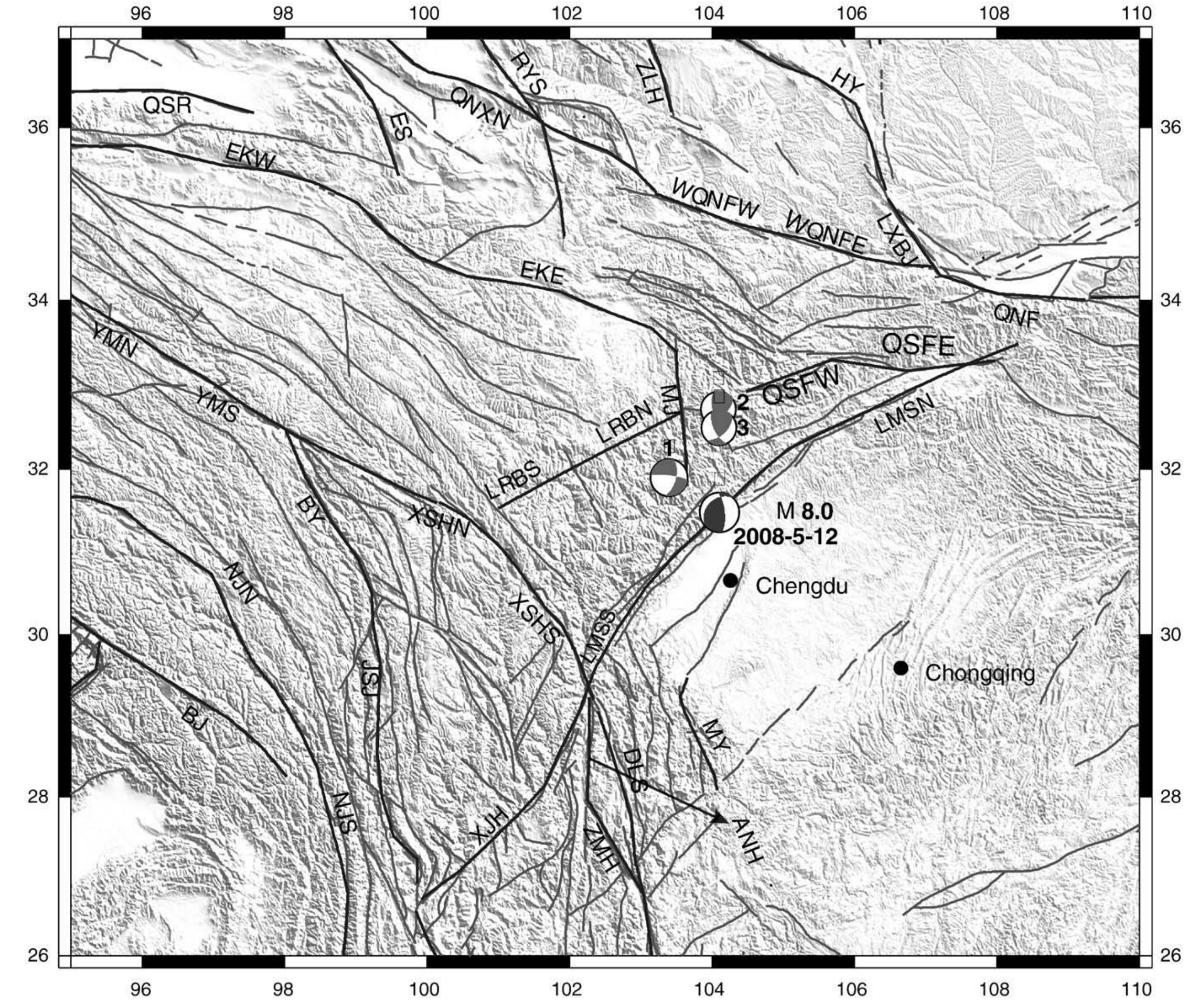

Fig. 1. Tectonic setting of the Wenchuan earthquake. Beach balls are earthquake focal mechanisms (lower hemisphere projection), the 1933 Diexi and 1976 Songpan doublet earthquakes are marked as nos. 1, 2, and 3, respectively. The thick black lines are active faults on which the Δ*CFS*s are investigated. Abbreviations of fault names are listed in Table 1.

which manifests the orogenic process of the Longmen Shan range, is believed to have started in Cretaceous time, and reactivated in the Paleocene and has been deforming since (Burchfiel et al., 1995). Recent GPS studies detected about 1.5 mm/yr shortening across the fault (Wang et al., 2008b), but only about 10 km of total slip has been accumulated geologically since its inception (Burchfiel et al., 1995).

The changes of Coulomb failure stress (*CFS*) induced by large earthquakes and their triggering effect to subsequent earthquakes have caught wide spread attention in recent years (e.g., Harris, 1998; Stein, 1999; Steacy et al., 2005; Gomberg and Felzer, 2008). Timely studies following large earthquakes illustrate the change of tectonic stresses in the vicinity and on fault, giving rise to the assessment of postseismic earthquake potential in the region. For example, McCloskey et al. (2005) computed the *CFS* changes after the 2004 Sumatra mega quake, and pointed out the substantial increase of *CFS* on the Nias–Simeulue section of the subduction zone. Three months later an Mw 8.7 quake struck that section of the thrust fault. Numerous *CFS* studies have been carried out after the Wenchuan earthquake. For example, Parsons et al. (2008) calculated *CFS* changes on faults in the vicinity of the Longmen Shan fault, particularly along the west and northwest rim of the Sichuan basin, and estimated the related earthquake probability. Toda et al. (2008) did a similar analysis for a larger region, with the geometries and senses of motion of regional faults determined from geological studies. While these studies have helped us gain much understanding of the regional stress changes and their associated change of seismic hazard potentials, they are sometimes subject to errors resulted from incomplete and inaccurate information about regional tectonic setting, geological fault parameters, and/or early earthquake source models. This study is to use an updated earthquake source model and a set of updated fault geometry and kinematic parameters to attempt a better assessment of the earthquake potentials in the region.

2. Evaluating *CFS* change

Earthquakes are produced by dislocation of rocks in the lithosphere. During an earthquake and within a short postseismic time period, the physical process in the vicinity of rupture zone is dominated by elastic deformation and release of elastic energy. To a first order approximation, we can use a uniform isotropic elastic half-space to simulate the Earth's media; and if the geometry of the fault

Please cite this article as: Wan, Y., Shen, Z.-K., Static Coulomb stress changes on faults caused by the 2008 Mw 7.9 Wenchuan, China earthquake, Tectonophysics (2010), doi:10.1016/j.tecto.2010.03.017

Table 1
Fault geometric parameters, Δ*CFS*, and recurring time change.

Fault	Abbreviation	No. of segments	Average strike (°)[a]	Dip (°)	Rake (°)	Shear stress (10^3 Pa)	Normal stress (10^3 Pa)	Δ*CFS* (10^3 Pa)	Average Δ*CFS* (10^3 Pa)	Time advance (year)[b]	Slip rate (m/yr), reference
Qaidam Southern Rim	QSR	5	91	45	90	−0.29 to −0.16	−0.15–0.04	−0.27 to −0.22	−0.25		
Ela Shan	ES	3	133	65	180	−0.12–0.97	−0.46 to −0.40	−0.30–0.79	0.33		
Qinghai Nanshan–Xunhua Nanshn	QNXN	9	111	90	180	0.92–1.34	0.05–1.36	0.94–1.89	1.49		
Riyue Shan	RYS	5	340	75	180	−0.79–1.34	−1.39 to −0.23	−0.91–0.79	0.34		
Zhuanglanghe	ZLH	2	348	90	180	−0.85 to −0.54	−0.34 to −0.10	−0.99 to −0.58	−0.78		
Haiyuan	HY	6	120	70	15	−1.62 to −0.51	−2.24 to −0.77	−2.91 to −0.95	−1.53		
West Qinling Northern Frontal (West)	WQNFW	4	93	60	15	−3.07 to −0.60	−7.52–1.17	−4.79 to −0.13	−2.81	−5.0 to −1.0	1.3 (Wang et al., 2010)
West Qinling Northern Frontal (East)	WQNFE	4	93	60	15	0.31–6.14	−10.2 to −1.32	−3.64–3.84	0.82	0.5–9.8	1.3 (Wang et al., 2010)
Qinling Southern Frontal West	QSFW	2	265	75	80	79.6	−133	26.3	26.3		
Qinling Southern Frontal (East)	QSFE	1	272	75	80	−2.38–5.93	1.35–2.15	−1.84–6.79	2.48		
Longxian–Baoji	LXBJ	2	97	45	45	4.37–4.39	−2.34 to −2.61	3.32–3.45	3.39		
Qinling Northern Frontal	QNF	3	299	70	−45	−1.55–1.05	0.48–1.03	−1.34–1.24	−0.32		
East Kunlun (West)	EKW	8	104	70	15	−0.08–1.04	−1.15–0.21	−0.46–1.03	0.56	0.0–0.2	11 (van der Woerd et al., 2002)
East Kunlun (East)	EKE	6	108	70	15	2.83–10.41	−0.59–6.49	2.63–13.0	8.24	1.5–5.5	4 (Kirby et al., 2007)
Longmen Shan (NE)	LMSN	5	265	90	180	3.46–87.9	−80.6 to −1.47	2.87–55.6	18.0	9.1–230	0.8 (Shen et al., 2009)
Longmen Shan (SW)	LMSS	2	241	43	90	8.04–26.1	−4.27 to −1.56	7.42–24.4	15.9	12.0–39.0	1.4 Shen et al., 2009
Minjiang (North)	NMJ	3	357	75	45	−35.3 to −4.36	−6.65–26.4	−24.8 to −7.02	−14.8	−39.0 to −4.8	1.9 (Wang et al., 2010)
Minjiang (South)	SMJ	2	357	75	45	−168 to −99.8	104–442	−58.2–8.98	−24.6	−185 to −110	1.9 (Wang et al., 2010)
Longriba (NE)	LRBN	2	50	90	180	−57.5 to −30.0	124–150	2.72–19.8	11.3	−18.0 to −9.4	6.7 (Wang et al., 2010)
Longriba (SW)	LRBW	2	50	90	180	−62.9 to −23.5	11.7–80.9	−30.5 to −18.8	−24.7	−19.7 to −7.3	6.7 (Wang et al., 2010)
Yushu–Maqu (NW)	YMN	5	297	75	0	−0.82 to −0.22	−0.17 to −0.05	−0.84 to −0.27	−0.47	−0.1–0	13 (Wang et al., 2008b)
Yushu–Maqu (SE)	YMS	4	297	75	0	−4.29 to −1.03	−0.08–0.30	−4.17 to −1.06	−2.40	−0.7 to −0.2	13 (Wang et al., 2008b)
Xianshuihe (N)	XSHN	2	326	90	0	−12.7 to −7.84	2.84–13.1	−7.49 to −6.71	−7.10	−2.7 to −1.6	10 (Shen et al., 2005)
Xianshuihe (S)	XSHS	4	326	90	0	−9.77–7.42	−3.17–28.7	0.98–13.5	7.90	−2.0–1.6	10 (Shen et al., 2005)
Nujiang (N)	NJN	11	326	45	90	−0.10 to −1.17	−0.20–0.74	−0.87 to −0.18	−0.54		
Nujiang (S)	NJS	5	326	45	90	−0.03–0.27	−0.12–0.05	−0.01–0.22	0.13		
Baiyu	BY	4	338	75	180	−0.05–2.03	2.74–4.98	1.94–3.61	2.94		
Jinshajiang	JSJ	8	351	75	180	−2.53–0.04	−0.57–3.06	−1.75 to −0.19	−0.91		
Bangongcuo–Jiali	BJ	6	307	75	135	−0.25–0.23	0.53–0.91	0.04–0.50	0.37		
Mabian–Yanjin	MY	6	91	90	0	−0.07–1.83	−8.74 to −1.74	−3.56–0.28	−0.46		
Xiaojinhe	XJH	8	36	75	0	−1.35 to −0.04	−4.51 to −0.26	−3.16 to −0.22	−0.96		
Daliangshan	DLS	7	349	75	0	−0.43–0.77	−7.58 to −0.50	−2.26 to −0.14	−0.96		
Anninghe	ANH	2	1	90	45	−0.59 to −0.32	−3.87 to −2.06	−2.13 to −1.14	−1.64		
Zemuhe	ZMH	2	340	65	45	0.34–0.52	−1.15 to −0.63	0.06–0.09	0.08		

[a] Fault strikes are measured from the corresponding segments shown in Fig. 1.
[b] Advance/delay time estimated based on shear stress change on fault.

and amount of slip are known, the displacement and strain fields within the Earth's media can be calculated from the dislocation theory (Chinnery, 1963; Okada, 1992). In this study we adopt the formulae and computing code summarized and provided by Okada (1992) to forward predict the static stress and strain field produced by the Wenchuan earthquake. The media property is prescribed as 3×10^{10} Pa for shear modulus and 0.25 for passion ratio.

From the Coulomb friction law, the ΔCFS on a fault interface is defined as:

$$\Delta CFS = \Delta\tau_s + \mu(\Delta\sigma_n + \Delta p) \tag{1}$$

where $\Delta\tau_s$ is the change of shear stress, $\Delta\sigma_n$ the change of normal stress (positive for extension), μ the effective friction coefficient, and Δp the

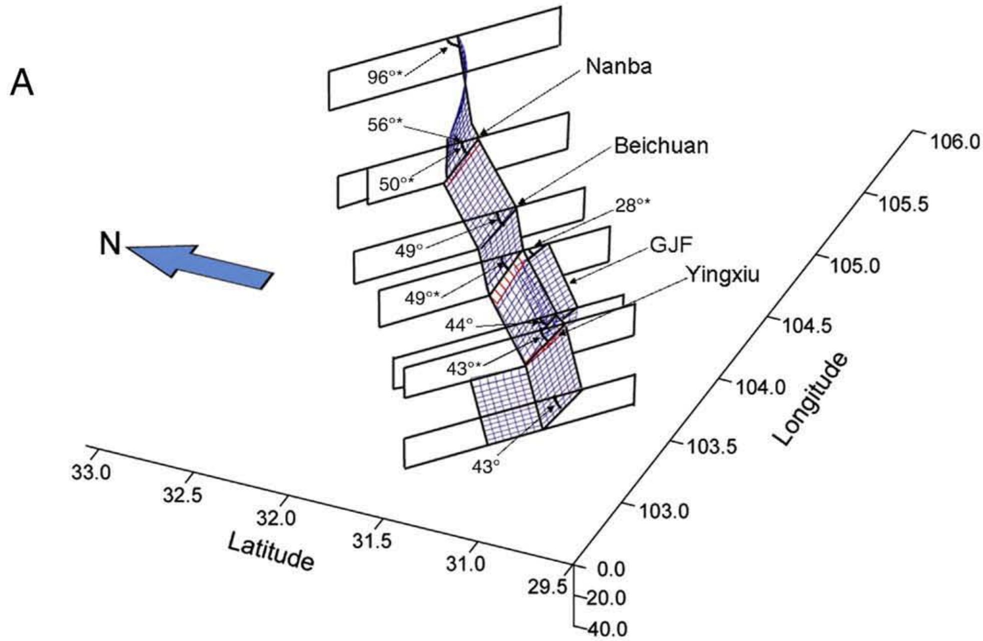

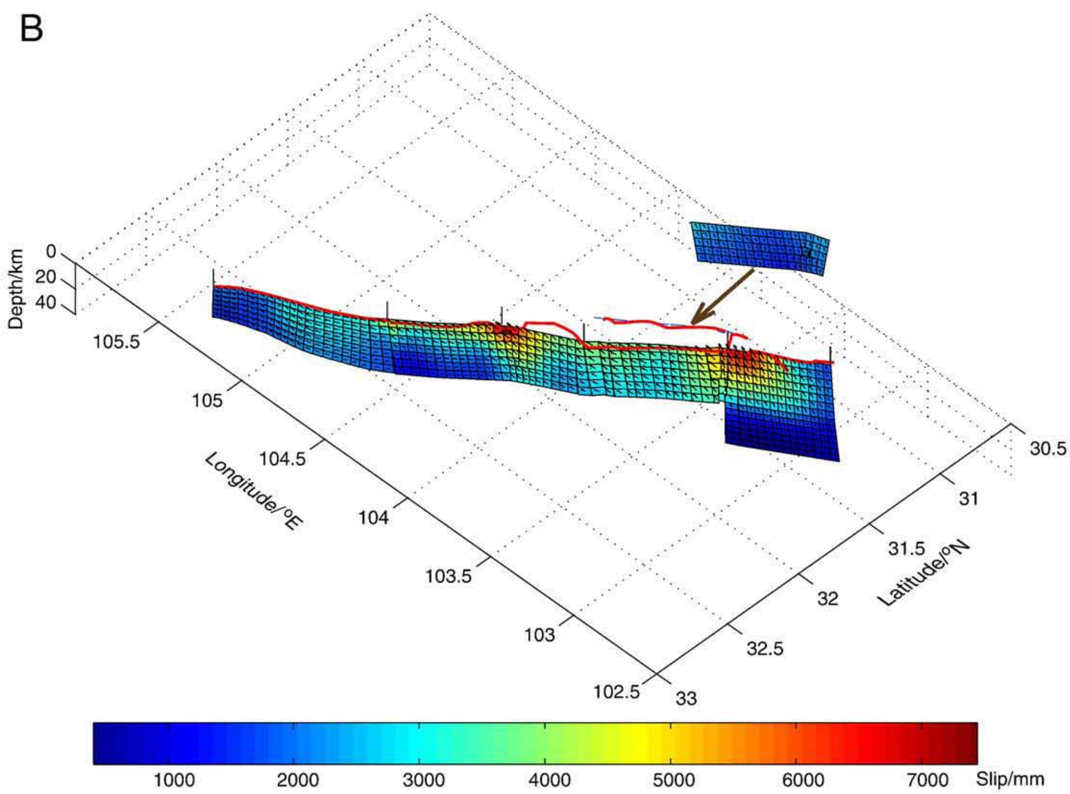

Fig. 2. Coseismic slip distribution of the Wenchuan earthquake and fault geometry of Shen et al. (2009). A) Fault geometry. The fault planes are viewed from southwest, at 45° elevation angle. Fault dip angle is assumed constant along dip and varies linearly along strike, with six dip angles at fault nodal points inverted in the solution (marked with a "*" sign). B) Coseismic slip distribution. The fault planes are viewed from northwest, at 45° elevation angle. The Guanxian–Jiangyou fault is plotted away from its original location (whose surface trace is marked as a blue line) to avoid image overlap. White arrows show the slip vectors on the fault patches, whose amplitudes are denoted by the colors of the patches.

change of pore pressure (Stein et al., 1992; King et al., 1994). The effect of friction reduction due to pore pressure can be represented by an equivalent friction coefficient $\mu' = \mu(1 - B)$, in which B is the Skempton coefficient, in the range of 0–1 (Rice, 1992). Eq. (1) therefore becomes:

$$\Delta CFS = \Delta\tau_s + \mu'\Delta\sigma_n \tag{2}$$

In our calculation we project the earthquake induced stress change first onto a fault plane, then to the slip direction of that fault. The ΔCFS is positive if it is in alignment with the fault slip direction, and vice versa. The slip directions of the fault segments are adopted from Deng et al. (2007). We assume $\mu' = 0.0$, 0.4, and 0.8 and evaluate the ΔCFS on faults, and assess how variation of this parameter would affect the results. The result will show that the calculated ΔCFS is sensitive to the choice of μ' for faults bearing large normal stress induced by the rupture of the Wenchuan earthquake. We finally assess seismic potential changes on faults associated with Coulomb stress variations induced by the earthquake, in terms of advancing and delay times of earthquake recurrence.

3. Regional fault kinematic and earthquake source models

3.1. Regional stress orientation and fault model

To compute the *CFS* changes on faults one needs to know the geometry and kinematics of the regional faults first. We adopt a fault model acquired mainly using geological and seismological information. Deng et al. (2007)

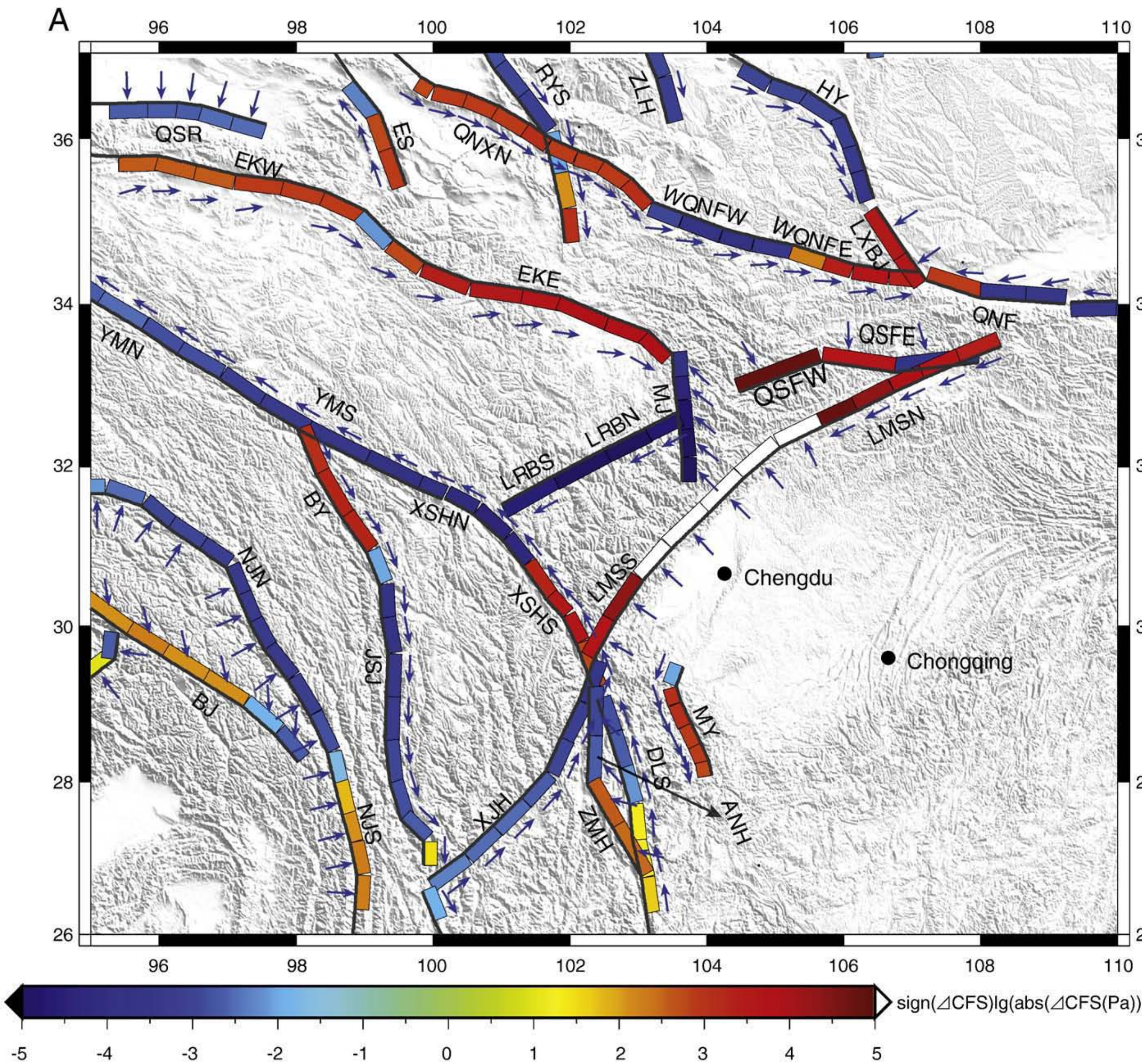

Fig. 3. ΔCFS caused by the Wenchuan earthquake and projected on fault plane and slip direction of the surrounding active faults at 10 km depth. (A), (B), and (C) are ΔCFS measured assuming apparent friction coefficient $\mu' = 0.0$, 0.4, and 0.8, respectively. (A) is also the shear stress $\Delta\tau_s$ projected on fault plane and slip direction. Colors between blue and green stand for decrease, and between red and green for increase of ΔCFS, respectively. The colors are in logarithmic scale of the absolute ΔCFS. Negative scale stands for decrease, and positive scale for increase of ΔCFS, respectively. Senses of fault slip directions are denoted by blue arrows: thrust and normal faults are indicated by arrows pointing to and away from the patches, respectively; fault parallel components of the arrows mark the motion directions of the strike-slip components. Thick black lines on the rims of the fault patches denote the locations of fault traces. Abbreviations of fault names are listed in Table 1. (For interpretation of the references to color in this figure legend, the reader is referred to the web version of this article.)

Please cite this article as: Wan, Y., Shen, Z.-K., Static Coulomb stress changes on faults caused by the 2008 Mw 7.9 Wenchuan, China earthquake, Tectonophysics (2010), doi:10.1016/j.tecto.2010.03.017

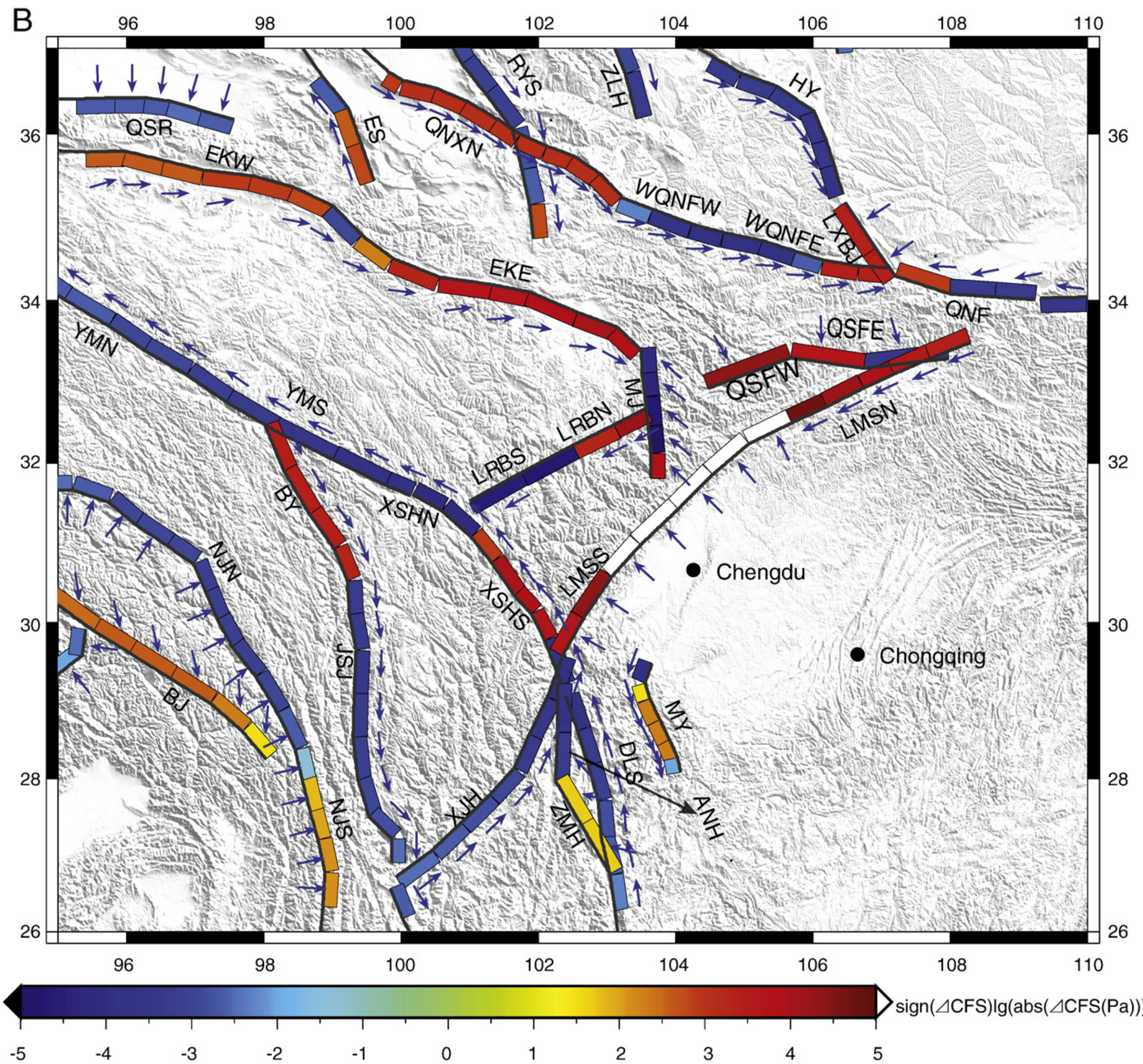

Fig. 3 (*continued*).

provided a dataset for the fault geometries in the region and some preliminary analysis of the regional fault kinematics. We employ their fault geometry parameters of surface locations and dip angles in the region with some simplification. Only the faults whose GPS estimated slip rates are greater than 1 mm/yr (Wang et al., 2008b, estimated from a 1999–2004 dataset) or those that are known to have been struck by large earthquakes historically (Molnar et al., 1984) are included. In addition, we also include the Longriba fault which Shen et al. (2005), Xu et al. (2008), and Wang et al. (2008b, 2010) found quite active, deforming right laterally at a rate of 4–7 mm/yr. We do not calculate the Δ*CFS* on the central part of the Longmen Shan fault which ruptured during the Wenchuan earthquake. Geometrical and kinematic parameters of the faults are listed in Table 1.

3.2. Earthquake mechanism and source model

The focal mechanism of the Wenchuan earthquake has been derived by the Harvard, China Earthquake Administration (CEA), and USGS groups using various datasets. All of the mechanism solutions describe a reverse faulting event with a right-lateral slip component. Besides the focal mechanism solutions, the slip distribution on fault has been investigated by numerous groups (Ji and Hayes, 2008; Nishimura and Yagi, 2008; Wang et al., 2008a; Hao et al., 2009; Kobayashi et al., 2009; Shen et al., 2009; Zhang et al., 2009). Despite the differences in details, all the models suggest a predominant unilateral slip progressed from southwest to northeast, and the southwest section was dominated by thrust and the northeast section by right-lateral faulting, respectively.

In this study we use a model constrained using GPS and InSAR data (Shen et al., 2009), which solved for slip distribution as well as fault geometry (Fig. 2). This model has better resolution on these parameters than previous studies due to model constraints using local geodetic data. Impact of postseismic deformation to coseismic slip estimation is believed to be rather minor (Shen et al., 2009), and not accounted for in this study. The model shows that from southwest to northeast the fault geometry changes progressively from moderately northwest dipping to

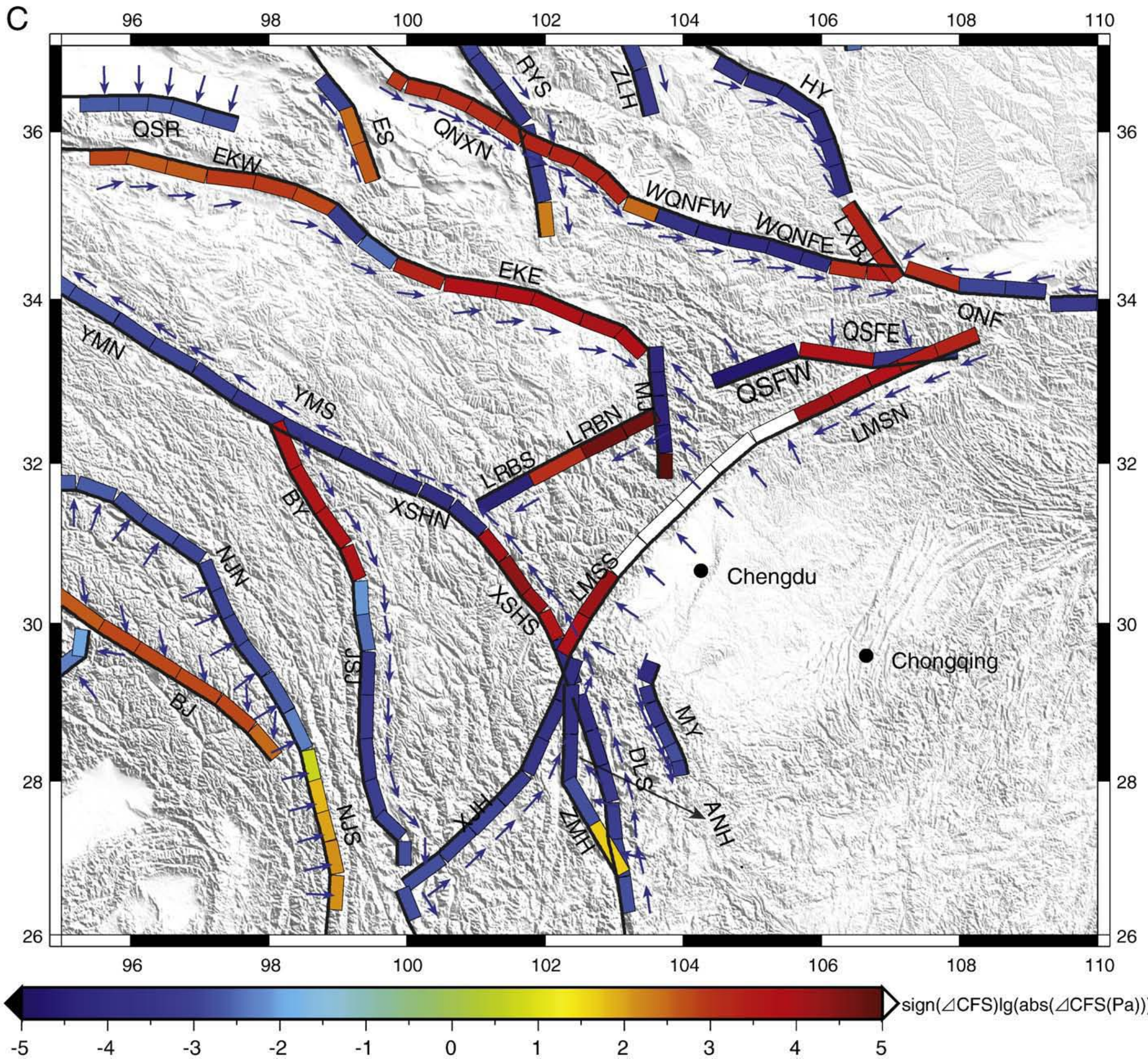

Fig. 3 (*continued*).

near vertical, and the rupture changes from predominantly thrust to right-lateral faulting. The rupture peaks at two places at shallow depth, one is near Yingxiu with about 5.8 m maximum reverse faulting, and the other near Beichuan with a maximum of about 5.0 m and 4.8 m reverse and dextral faulting, respectively. The released moment is 7.3×10^{20} N-m, equivalent to M_w 7.9. Using this model the stress change at each of the receiver fault planes caused by the coseismic slip on the Wenchuan fault is calculated, and then converted to ΔCFS for further study. We choose the ΔCFS at 10 km fault depth for evaluation, since most of the earthquakes in the region occurred in the depth range of 0–25 km (Zhu et al., 2005).

4. Results and discussions

4.1. ΔCFS estimation results

The primary driving force of fault rupture is the shear stress imposed on the fault plane. The normal stress, depending on the effective friction coefficient, may play an important role in dictating the failure state of a fault. To illustrate how the shear and normal stress changes on faults manifest the ΔCFS we calculate the two components at the depth of 10 km and plot the results in Figs. 3A and 4A. The shear stress changes on faults projected to the fault slip direction are also the ΔCFS per $\mu' = 0.0$. The active faults whose earthquake induced shear stresses increased are the south and north segments of the Longmen Shan, west part of the Qinling Southern Frontal, east segment of the West Qinling Northern Frontal, Longxian–Baoji, south segment of the Xianshuihe, Baiyu, most part of the Mabian–Yanjin, Qinghai Nanshan–Xunhua Nanshan, East Kunlun, south part of the Ela Shan, Zemuhe, west part of the Bangongcuo–Jiali, and south segment of the Nujiang faults (Fig. 3A). The faults whose earthquake induced shear stresses (i.e. ΔCFS when $\mu' = 0.0$) increased for more than 10^4 Pa are: the south and north segments of the Longmen Shan (up to 2.6×10^4 Pa and 8.8×10^4 Pa), west segment of the Qinling Southern Frontal (up to 8.0×10^4 Pa), and east segment of the East Kunlun (up to 1.0×10^4 Pa) faults. The active faults whose earthquake induced shear stresses decreased are the Minjiang, Longriba, Haiyuan, Yushu–Maqu,

Please cite this article as: Wan, Y., Shen, Z.-K., Static Coulomb stress changes on faults caused by the 2008 Mw 7.9 Wenchuan, China earthquake, Tectonophysics (2010), doi:10.1016/j.tecto.2010.03.017

north segment of the Xianshuihe, north segment of the Nujiang, north part of the Daliangshan, north part of the Riyue Shan, Qaidam Southern Rim, Zhuanglanghe, Xiaojinhe, and Anninghe faults. The faults whose shear stresses decreased more than 10^4 Pa are: the Minjiang (up to 1.7×10^5 Pa), Longriba (up to 6.3×10^4 Pa), and north segment of the Xianshuihe (up to 1.3×10^4 Pa) faults.

If $\mu'\neq0$, the normal stresses on faults will contribute to the ΔCFS. The active faults whose earthquake induced normal stresses increased (*i.e.* corresponding to increases of ΔCFS) are the Longriba, south segment of the Minjiang, most part of the Xianshuihe, Baiyu, central part of the Nujiang, Bangongcuo–Jiali, east segment of the East Kunlun, Qinghai Nanshan–Xunhua Nanshan, Qingling Northern Frontal, and the east segment of the Qinling Southern Frontal faults (Fig. 4A). The faults whose normal stresses increased more than 10^4 Pa are: the Longriba (up to 1.5×10^5 Pa), south part of the Minjiang (up to 4.4×10^5 Pa), Central part of the Xianshuihe (up to 2.9×10^4 Pa) faults. The active faults whose normal stresses decreased (i.e. corresponding to decreases of ΔCFS) are: the north and south segments of the Longmen Shan, northernmost part of the Minjiang, central part of the East Kunlun, east part of the Qaidam Southern Rim, Ela Shan, Riyue Shan, Zhuanglanghe, Haiyuan, Longxian–Baoji, east segment of the West Qinling North Frontal, west segment of the Qinling Southern Frontal, south part of the Nujiang, most part of the Jinshajiang, Xiaojinhe, Anninghe, Daliangshan, and Mabian–Yanjin faults. The faults whose normal stresses decreased more than 10^4 Pa are: the west segment of the Qinling Southern Frontal (up to 1.3×10^5 Pa), northeast segment of the Longmen Shan (up to 8.1×10^4 Pa), and west part of the Qinling Northern Frontal (up to 1.0×10^4 Pa) faults.

The calculated *CFS* changes under the assumption of $\mu'=0.4$ are shown in Fig. 3B. The active faults with *CFS* increased greater than 10 Pa

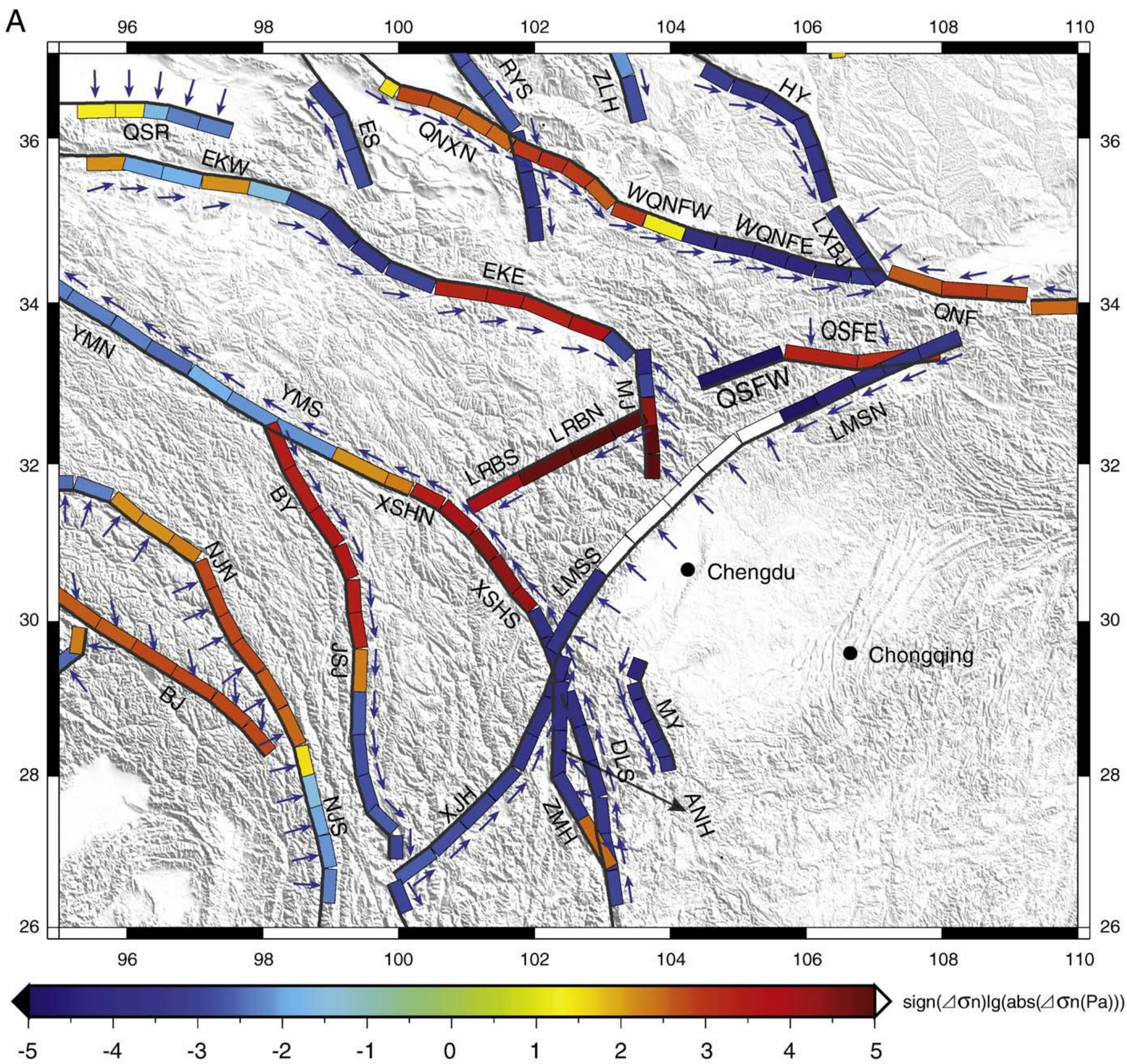

Fig. 4. (A) Normal stress $\Delta\sigma_n$ induced by the Wenchuan earthquake. (B) ΔCFS differences on faults between the results calculated assuming apparent friction coefficients of 0.4 and 0.0 or 0.8 and 0.4. All the results are evaluated on fault planes at 10 km depth. Thick black lines on the rims of the fault patches denote the locations of fault traces. Abbreviations of fault names are listed in Table 1.

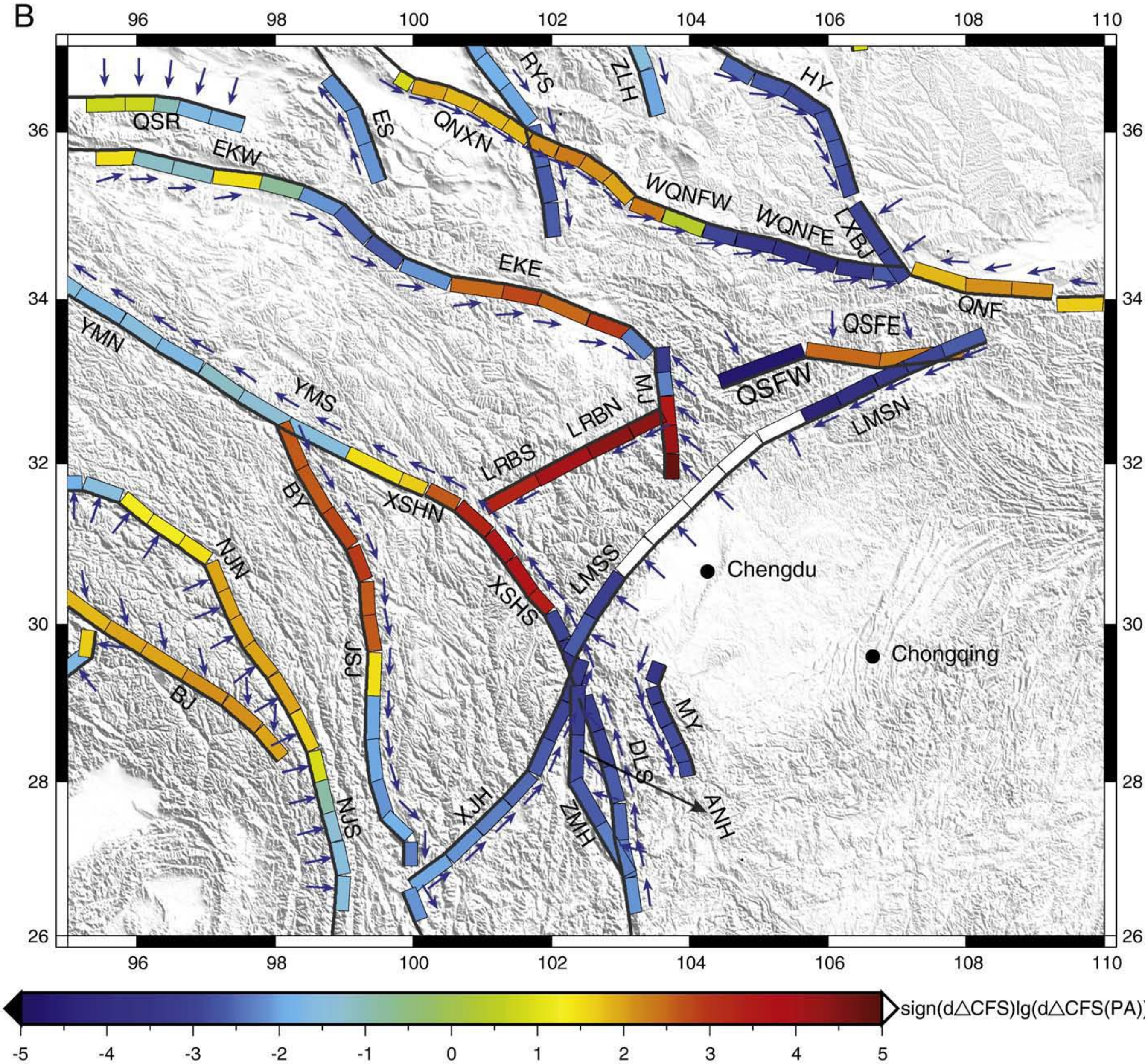

Fig. 4 (*continued*).

are distributed in the northeast, northwest, and southwest of the fault rupture. They are the southeast segment of the Xianshuihe, northern part and southern most part of the Longmen Shan, East Kunlun, Longxian–Baoji, Ela Shan, Baiyu, southernmost part of the Riyue Shan, central part of the Mabian–Yanjing, Bangongcuo–Jiali, Zemuhe, south segment of the Nujiang, and Qinghai Nanshan–Xunhua Nanshan faults. The faults whose *CFS*s increased significantly are: the southwest and northeast parts of the Longmen Shan (2.4×10^4 and 5.6×10^4 Pa), west segment of the Qinling Southern Frontal (2.6×10^4 Pa), southeast part of the East Kunlun (1.3×10^4 Pa), east segment of the Longriba (2.0×10^4 Pa), south segment of the Xianshuihe (1.4×10^4 Pa), southernmost part of the Minjiang (9.0×10^3 Pa), Baiyu (3.0×10^3 Pa), west segment of the West Qinling Northern Frontal (3.8×10^3 Pa), and Longxian–Baoji (3.5×10^3 Pa) faults. Special attention should be paid to the seismic activities on these faults. The regional faults with more than 10 Pa of relaxed *CFS* are the west segment of the Longriba, north segment of the Nujiang, west segment of the West Qinling Northern Frontal, Qinling Northern Frontal, Zhuanglanghe, northern part of the Riyue Shan, Haiyuan, north part of the Minjiang, Yushu–Maqu, Jinshajiang, Xiaojinhe, Anninghe, and Daliangshan faults. The faults with significantly *CFS* relaxation are the most part of the Minjiang and west part of the Longriba faults, with the *CFS* decreased up to 5.8×10^4 and 3.1×10^4 Pa, respectively (Table 1).

Fig. 4B shows the differences of the two Δ*CFS* results: Δ*CFS* ($\mu'=0.4$)−Δ*CFS* ($\mu'=0.0$). Examination of the result reveals that significant changes are along these faults which gain large increase of normal stress: the Longriba, south part of the Minjiang, and central part of the Xianshuihe faults, resulting in Δ*CFS* changing from negative to positive along the east segment of the Longriba, southernmost part of the Minjiang, and a portion of the central segment of the Xianshuihe faults. On the other hand, some faults have their normal stresses and Δ*CFS*s decreased, such as the northeast and southwest segments of the Longmen Shan, west segment of the Qinling Southern Frontal, and east segment of the West Qingling Northern Frontal faults. A portion of the

Please cite this article as: Wan, Y., Shen, Z.-K., Static Coulomb stress changes on faults caused by the 2008 Mw 7.9 Wenchuan, China earthquake, Tectonophysics (2010), doi:10.1016/j.tecto.2010.03.017

east segment of the West Qinling Northern Frontal fault even has the sense of its Δ*CFS* reversed, from positive to negative.

We test another case of apparent friction coefficient assuming $\mu' = 0.8$, and evaluate the Δ*CFS*s on fault planes at 10 km depth. Fig. 3C shows the Δ*CFS* result. Comparing the Δ*CFS* estimates assuming $\mu' = 0.8$ with that of $\mu' = 0.4$ (Fig. 3C vs. Fig. 3B), we find that most of Δ*CFS* estimates do not change much, or at least the senses of Δ*CFS* are not changed. Nevertheless, faults located close to earthquake rupture and with large changes of normal stress demonstrate noticeable differences in Δ*CFS*. Greater μ' means higher weighting of normal stress in Δ*CFS* evaluation, resulting in escalating the Δ*CFS* on the Longriba fault, and transforming the Δ*CFS* on the central segment of the fault from negative to positive. The Δ*CFS* on the southernmost part of the Minjiang fault is also increased significantly. The Δ*CFS* on the west segment of the Qinling Southern Frontal fault, on the other hand, changes from positive to negative. Causes of these changes are the differential normal stresses between the two cases, which are identical to the differences between two cases of $\mu' = 0.0$ and 0.4, as shown in Fig. 4B.

We also calculate the Δ*CFS*s evaluated at 5 km and 15 km depth, and compare that against the one evaluated at 10 km depth, all assuming the same effective friction coefficient of 0.4 (Fig. 5A–D). Comparing Fig. 3B with Fig. 5A and C, we can see that the senses of Δ*CFS*s do not vary with depth, and values of Δ*CFS*s have only slight variations which decay with distance from the source (Fig. 5B and D). The maximal variations of Δ*CFS* are at the NW and SE ends of the Wenchuan rupture on the Longmen Shan, southernmost part of the Minjiang, and west segment of the Qinling Southern Frontal faults, where the Δ*CFS*s at 5 km depth differ by 1.9×10^3 Pa, 9.5×10^2 Pa, -3.8×10^4 Pa, -1.3×10^4 Pa from that measured at 10 km depth, and the same as the Δ*CFS*s measured at 15 km depth but with opposite

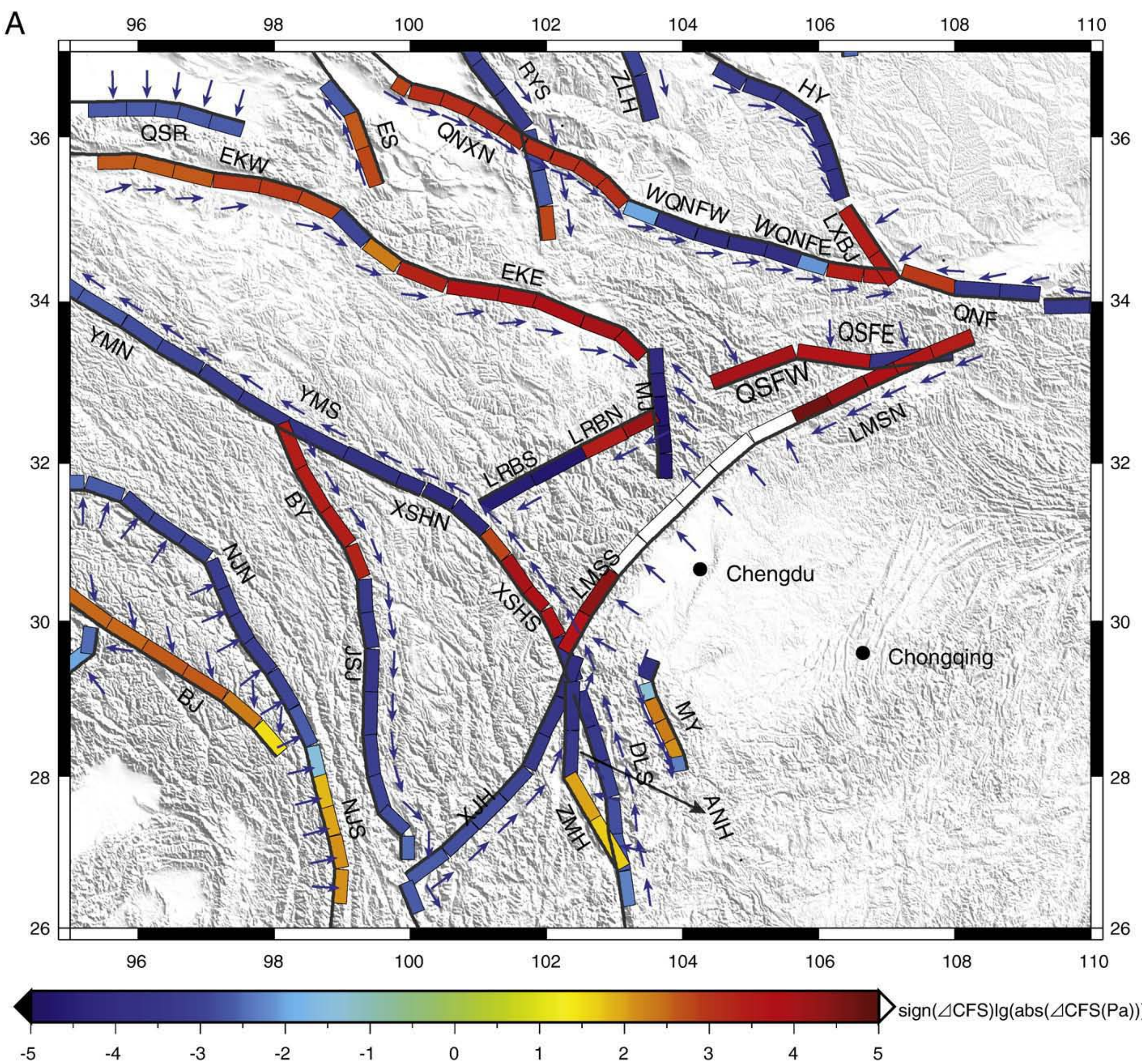

Fig. 5. (A) and (C): Δ*CFS* result on faults calculated at 5 and 15 km depths respectively. (B) and (D): Δ*CFS* differences on faults between the results calculated at 5 and 10 km depths and 15 and 10 km depths, respectively. All the results are evaluated assuming apparent friction coefficient of 0.4. Thick black lines on the rims of the fault patches denote the locations of fault traces. Abbreviations of fault names are listed in Table 1.

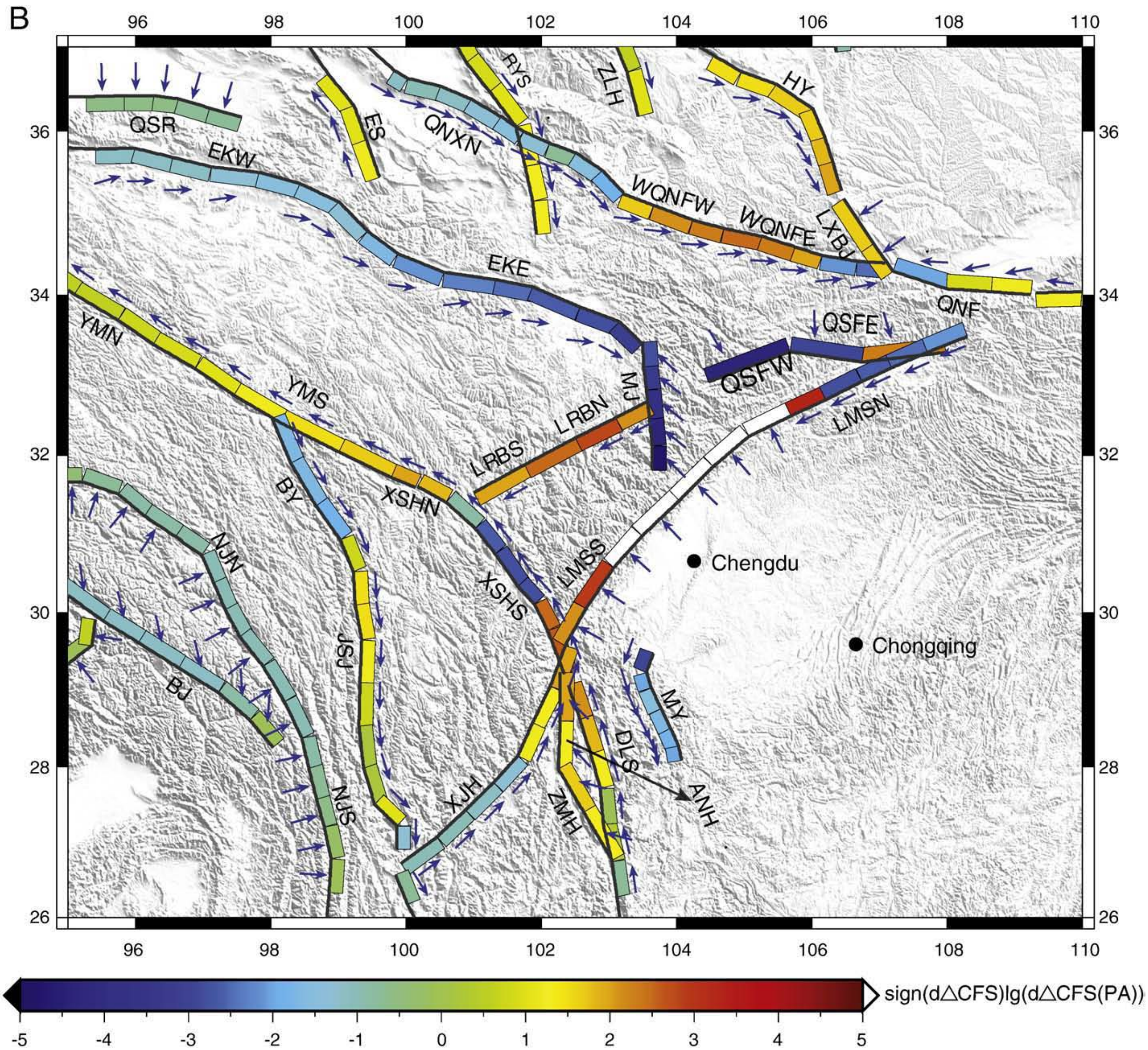

Fig. 5 (*continued*).

signs. We conclude that the ΔCFSs induced by the Wenchuan earthquake are pretty stable on most of the faults within depth range of the upper crust.

4.2. Advance/delay times of earthquake recurrence

Our next step is to convert the ΔCFS calculated on faults into assessments of their seismic potentials. Precise estimation of earthquake probabilities is difficult due to the lack of information about historical earthquake records, current levels of tectonic loading, and earthquake recurrence times. Nevertheless, using present day tectonic deformation rates we can convert the ΔCFS calculated on faults into advance/delay times to the next characteristic earthquake on the fault segments. Such assessments are done in three steps for a selection of faults, whose slip rates are known to be greater than 1 mm/yr. First, we obtain secular slip rates of these faults located in the southeast Tibetan plateau from Shen et al. (2005) and Wang et al. (2008b), and those in the northeast Tibetan plateau from Wang et al. (2010). Second, we convert the secular fault slip rates into strain accumulation rates on fault. This is done assuming that the faults are locked down to 20 km depth, and surface deformation is in the form of $D(x)=2\,S/\pi\,\mathrm{atan}(x/H)$, where S is the slip rate beneath locking depth H. The shear strain rate at the surface is therefore $\dot{\varepsilon}=S/(\pi H)$, where $H=20$ km. Third, we convert the Coulomb stress change on each fault segment to strain change $\Delta Strian$ assuming linear elasticity, and estimate the earthquake advance/delay time of the fault using a formula $\Delta T=\Delta Strian/\dot{\varepsilon}$. It should be noted that the ΔCFS used in this calculation accounts for shear stress change only (i.e. $\mu'=0$), since the slip deficit accumulated on fault plane is associated with the shear stress and strain only. The derived earthquake advance/delay times are thus listed in Table 1.

Our result shows that the faults whose recurring times have been advanced the most are the SW and NE segments of the Longmen Shan fault, up to 39 and 230 years respectively. These results are

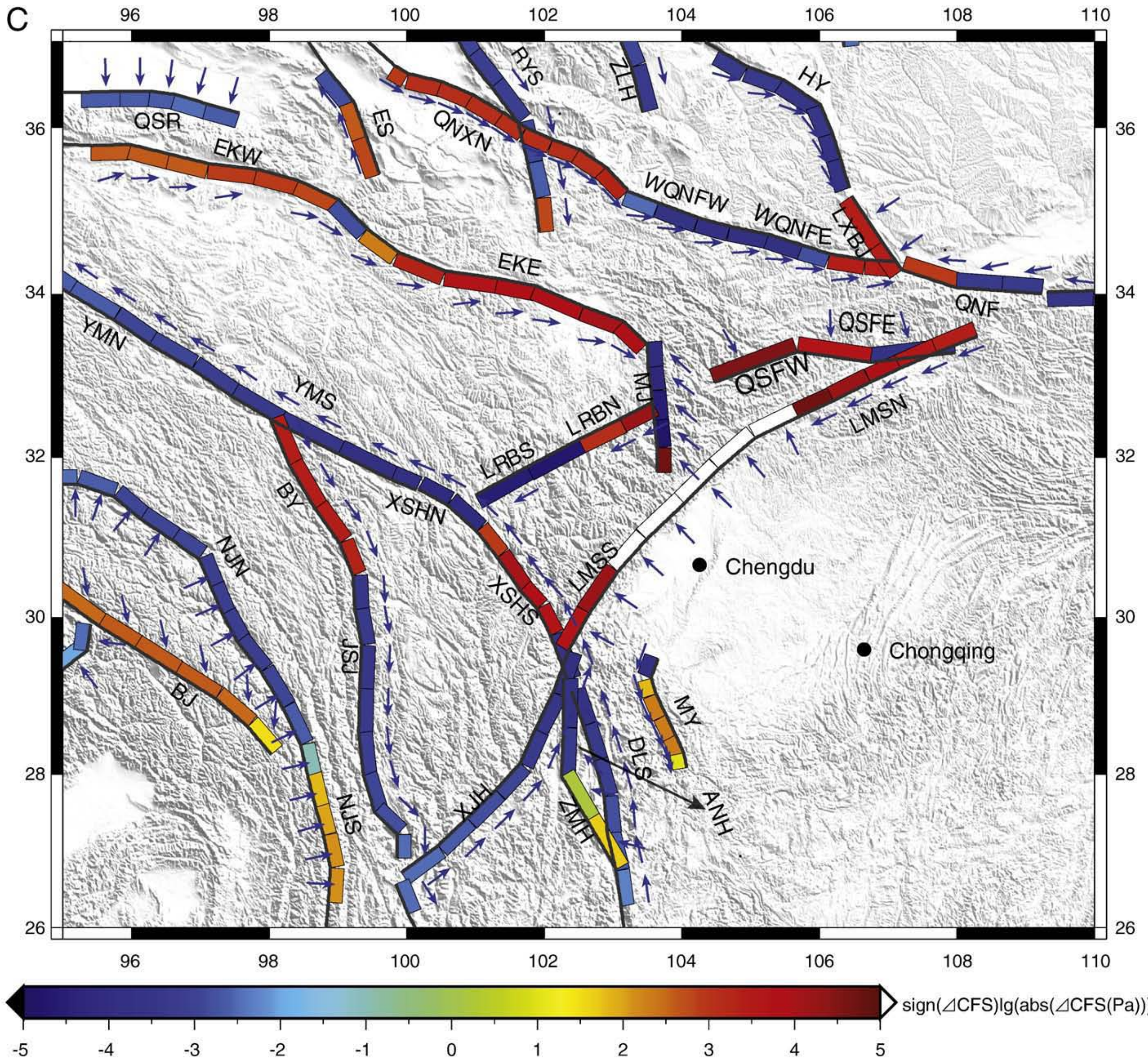

Fig. 5 (*continued*).

manifested mainly by two factors, one is the proximity of the faults to coseismic rupture, and the other their slow fault slip rates (1.4 mm/a and 0.8 mm/a for the dextral components respectively [Shen et al., 2009]). We have no precise estimates of earthquake recurrence time intervals for the two segments. Such estimate for the central segment of the Longmen Shan fault, however, is around 4000 years (Shen et al., 2009). The advancements of recurring times on the two faults segments therefore are probably only small fractions of the recurrence intervals. The fault segment toward east end of the East Kunlun fault has been affected noticeably, with advancing time of ~5.5 years. The effect on the Xianshuihe fault segments seems to be small, with recurring times advanced merely 1.6 years for the south segment. The faults which fall into stress shadows get their recurring times delayed, among which the most noticeable ones are: up to 185 years for the south segment of Minjiang fault, up to 18 years for the northeast segment of the Longriba fault, ~9.8 years for the west segment of Western Qinling Northern Frontal, and up to 2.7 years for the northwest segment of Xianshuihe fault, respectively.

4.3. Approximations and effects

We take a first order approximation in computing the effect of the ΔCFS at the surrounding faults, neglecting numerous second order effects. For example, we adopted an elastic half-space model in the ΔCFS calculation, ignoring effects caused by the layered Earth or even 3-D inhomogeneous structure. Errors produced by such an approximation are estimated as 10% or less for most cases (Savage, 1998). Negligence of strain diffusion after large earthquakes due to viscoelastic relaxation of the earth media will also result in errors, which, however, will only be much smaller than the coseismic effect during the first couple of years after the quake, for an asthenosphere whose viscosity is of 10^{19}–10^{21} Pa-s (Deng, et al., 1998; Shen et al., 2003; Wan et al., 2007). We also did not consider afterslip effect in this calculation, since its contribution is not significant comparing to that of mainshock (Shen et al., 2009). Most of the aftershock contributions have been accounted for implicitly. This is because the coseismic slip model (Shen et al., 2009) we adopted to compute

Please cite this article as: Wan, Y., Shen, Z.-K., Static Coulomb stress changes on faults caused by the 2008 Mw 7.9 Wenchuan, China earthquake, Tectonophysics (2010), doi:10.1016/j.tecto.2010.03.017

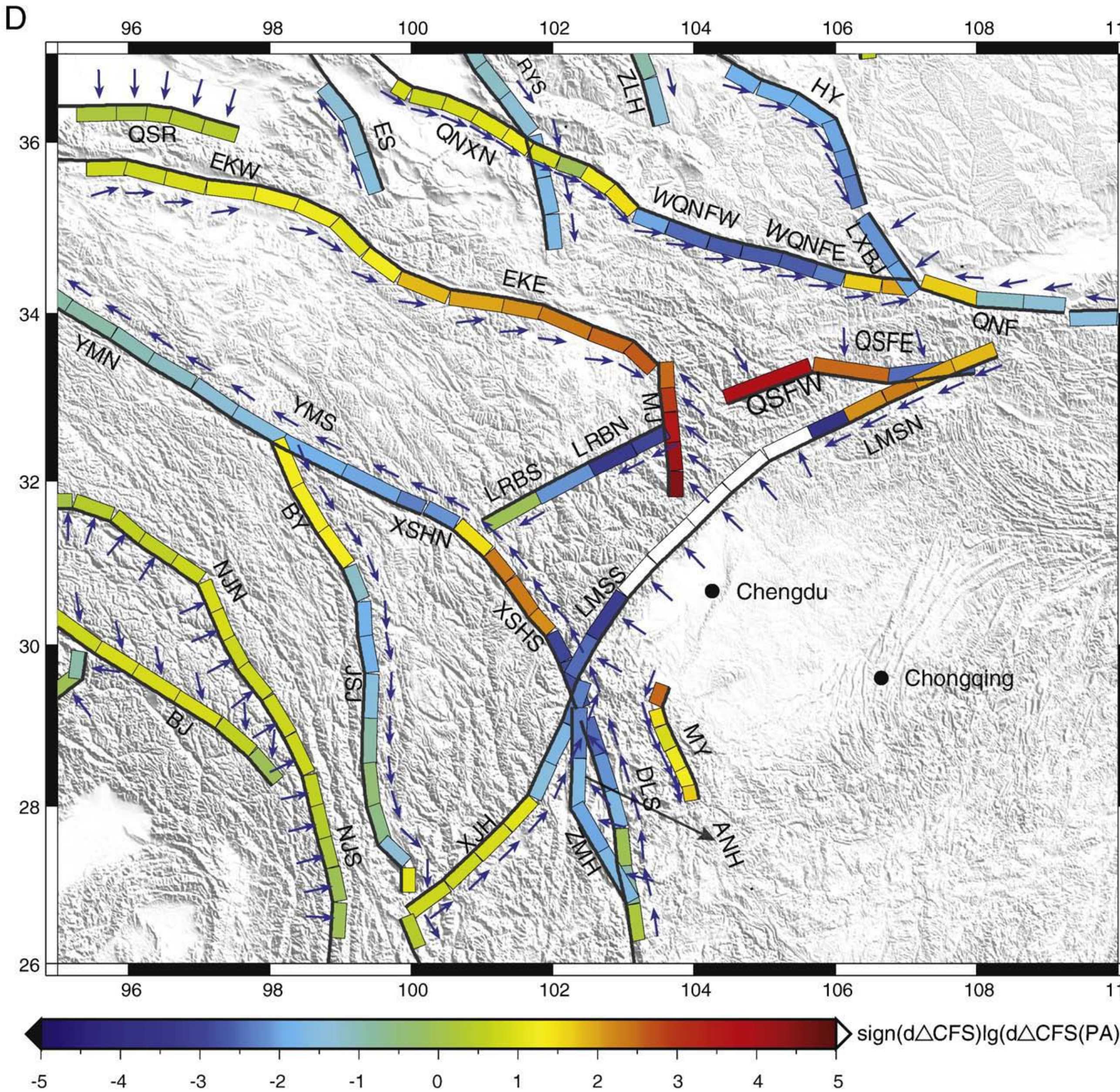

Fig. 5 (*continued*).

Coulomb stress changes was constrained by GPS and InSAR data which were collected a few weeks after the mainshock (e.g. the postseismic ALOS SAR measurements were made 24 to 48 days after the quake) by then most of the large aftershocks occurred already. Those aftershocks occurred in later times after the geodetic data collection (whose magnitudes are 6 or less) would result in regional stress changes which are much smaller than that predicted by our coseismic model. Taking all the approximations listed above into account, we conclude that their effects are relatively minor, and would not have major impact on our evaluation of the Δ*CFS* at the surrounding faults of the Wenchuan earthquake.

4.4. Comparisons with previous studies

To compare our result with previous studies, we find that our results are in general agreements with that of Parsons et al. (2008) and Toda et al. (2008). For example, both Parsons et al. (2008) and our study estimated *CFS* increase at the eastern end of the East Kunlun and southeastern Xianshuihe faults and stress shadow at the Minjiang fault. Nevertheless, our study area is larger than that of theirs, and our results provide assessments of Δ*CFS* at more regional faults. Comparing our results with that of Toda et al. (2008), we find very good agreement along most faults, such as increased Δ*CFS* on the southern and northern Longmen Shan, East Kunlun, southern Xianshuihe, and Qinling Southern Frontal faults, and decreased Δ*CFS* on the southern Minjiang, Longriba, and northern Xianshuihe faults. The only noticeable exception is at the northern Minjiang fault where our result shows the *CFS* decreased by up to 2.5×10^4 Pa, while theirs yields an increase as much as $\sim4\times10^4$ Pa (reading their Fig. 1A, Coulomb stress calculated using the Ji and Hayes' source model). Such a difference is quite remarkable, and is probably resulted from the difference in fault slip models used in the two studies. Both Toda et al. (2008) and our study adopted the result of Deng et al. (2007) to define fault models in Δ*CFS* computation. In our study we assume that the northern Minjiang fault strikes north and slip obliquely with compressional and sinistral components. At the location of the northern Minjiang fault (~103.5°E, 33.5°N), however, Toda et al. (2008) assumed a focal mechanism of predominantly left-slip on a vertical fault striking northwest. Such a focal mechanism differs significantly from the one we derived from Deng et al. (2007) on the fault, and is quite close to the focal mechanism at the eastern end of the East Kunlun fault located north of the Minjiang fault. Their result on the spot seems to be a prediction of ΔCFS along faults which are more East Kunlun like than Minjiang like.

The earthquake source models used in this study and Toda et al. (2008) are also somewhat different, and may be the source of more differences. Although both earthquake source models demonstrated two rupture maxima in the fault rupture plane, their spatial locations, however, differ by tens of kilometers. Another significant difference comes from the fault geometry model: the source models of Ji and Hayes (2008) and Nishimura and Yagi (2008) prescribed a constant dipping fault along strike, whereas those of Shen et al. (2009) allowed fault dip angle to vary along strike. As the fault dip angle in Shen et al.'s model increases progressively from southwest to northeast, the discrepancy also increases, up to >50° at the northeastern end of the fault rupture plane. As a result, the source model of Shen et al. (2009) would not allow much horizontal contraction across the northeastern end of the fault plane, therefore predicting less NW–SE extension in its neighborhood than other fault models would do. That should explain our estimate of ΔCFS ~2.6×10^4 Pa at the Southern Qinling Frontal fault, which is markedly less than the ~4.0×10^4 Pa estimate by Toda et al. (2008) on the same fault (reading from their Fig. 1A). The source model of Shen et al. (2009) was constrained using GPS, InSAR, and fault surface break measurements, and is regarded more accurate than other preliminary models derived quickly after the quake using teleseismic data only. Aftershock studies also show near vertical aftershock envelops across the northeast section of the fault, consistent with the estimate that the fault plane there is near vertical (Chen et al., 2009; Huang et al., 2008). Our study, using a revised source model therefore, may provide better estimates of ΔCFS at some regions than previous studies did. Such results are used to estimate changes of earthquake recurring times, enabling us to assess changes of seismic hazard potentials due to the Wenchuan earthquake along major faults located around the eastern rim of the Tibetan plateau and the western Sichuan basin.

Acknowledgments

We are grateful to Kelin Wang, two anonymous reviewers, and the chief editor of Tectonophysics for their comments and suggestions. This work was supported by grants from the Natural Science Foundation of China (40674022), the Ministry of Science and Technology (LED2008A05, 2008CB425703), the China Earthquake Administration (200808053), and NSF (0911762).

References

Burchfiel, B.C., Chen, Z., Liu, Y., Royden, L.H., 1995. Tectonics of the Longmen Shan and adjacent regions. Int. Geol. Rev. 37, 661–735.

Chen, J.H., Liu, Q.Y., Li, S.C., et al., 2009. Seismotectonic study by relocation of the Wenchuan Ms 8.0 earthquake sequence. Chinese J. Geophys. (in Chinese) 52 (2), 390–397.

Chinnery, M.A., 1963. The stress changes that accompany strike-slip faulting. Bull. Seismol. Soc. Amer. 53, 921–932.

Deng, J., Gurnis, M., Kanamori, H., Hauksson, E., 1998. Viscoelastic flow in the lower crust after the 1992 Landers, California, earthquake. Science 282, 1689–1692.

Deng, Q.D., et al., 2007. Active Tectonics Map of China. Seismological Press, Beijing.

Gomberg, J., Felzer, K., 2008. A model of earthquake triggering probabilities and application to dynamic deformations constrained by ground motion observations. J. Geophys. Res. 113, B10317. doi:10.1029/2007JB005184.

Hao, K.X., Si, H., Fujiwara, H., Ozawa, T., 2009. Coseismic surface-ruptures and crustal deformations of the 2008 Wenchuan earthquake Mw7.9, China. Geophys. Res. Lett. 36, L11303.

Harris, R.A., 1998. Introduction to special section, stress triggers, stress shadows, and implications for seismic hazard. J. Geophys. Res. 103, 24347–24358.

Huang, Y., Wu, J.P., Zhang, T.Z., Zhang, D.N., 2008. Relocation of the M8.0 Wenchuan earthquake and its aftershock sequence. Sci. China Ser. D 51 (12), 1703–1711.

Ji, C., Hayes, G., 2008. Preliminary Result of the May 12, 2008 Mw 7.9 Eastern Sichuan, China Earthquake. http://earthquake.usgs.gov/eqcenter/eqinthenews/2008/us2008ryan/finite_fault.php.

Kan, R., Zhang, S., Yan, F., Yu, L., 1977. Present tectonic stress field and its relation to the characteristics of recent tectonic activity in southwestern China. Acta Geophys. Sin. 20 (2), 96–109 in Chinese.

King, G.C.P., Stein, R.S., Lin, J., 1994. Static stress changes and the triggering of earthquakes. Bull. Seismol. Soc. Amer. 84, 935–953.

Kirby, E., Harkins, N., Wang, E., et al., 2007. Slip rate gradients along the eastern Kunlun fault. Tectonics 26 (TC2010).

Kobayashi, T., Takada, Y., Furuya, M., Murakami, M., 2009. Locations and types of ruptures involved in the 2008 Sichuan earthquake inferred from SAR image matching. Geophys. Res. Lett. 36, L07302.

McCloskey, J., Nalbant, S.S., Steacy, S., 2005. Earthquake risk from co-seismic stress. Nature 434, 291.

Molnar, P., Deng, Q., 1984. Faulting associated with large earthquakes and the average rate of deformation in central and eastern Asia. J. Geophys. Res. 89, 6203–6227.

Nishimura, N., Yagi, Y., 2008. Rupture Process for May 12, 2008 Sichuan Earthquake (Preliminary Result). http://www.geol.tsukuba.ac.jp/~nisimura/20080512/.

Okada, Y., 1992. Internal deformation due to shear and tensile faults in a half-space. Bull. Seismol. Soc. Amer. 82, 1018–1040.

Parsons, T., Ji, C., Kirby, E., 2008. Stress changes from the 2008 Wenchuan earthquake and increased hazard in the Sichuan basin. Nature. doi:10.1038/nature07177.

Rice, J.R., 1992. Fault stress states, pore pressure distribution, and the weakness of the San Andreas fault. In: Evans, B., Wong, T.F. (Eds.), Fault Mechanics and Transport Properties of Rock. Academic Press, London, pp. 475–503.

Savage, J.C., 1998. Effect of crustal layering upon dislocation modeling. J. Geophys. Res. 92, 10595–10600.

Shen, Z., Wan, Y., Gan, W., Zeng, Y., Ren, Q., 2003. Viscoelastic triggering between large earthquakes along the east Kunlun fault system. Chinese J. Geophys. 46 (6), 1125–1138.

Shen, Z., Lü, J., Wang, M., Bürgmann, R., 2005. Contemporary crustal deformation around the southeast borderland of the Tibetan Plateau. J. Geophys. Res. 110, B11409. doi:10.1029/2004JB003421.

Shen, Z.K., Sun, J., Zhang, P., Wan, Y., Wang, M., Bürgmann, R., Zeng, Y., Gan, W., Liao, H., Wang, Q., 2009. Slip maxima at fault junctions and rupturing of barriers during the 2008 Wenchuan earthquake. Nature Geoscience 2, 718–724. doi:10.1038/NGEO636.

Steacy, S., Gomberg, J., Cocco, M., 2005. Introduction to special section: stress transfer, earthquake triggering, and time-dependent seismic hazard. J. Geophys. Res. 110. doi:10.1029/2005JB003692 B05S01.

Stein, R.S., 1999. The role of stress transfer in earthquake occurrence. Nature 402, 605–609.

Stein, R.S., King, G.C.P., Lin, J., 1992. Change in failure stress on the southern San Andreas fault system caused by the 1992 magnitude = 7.4 Landers earthquake. Science 258, 1328–1332.

Toda, S., Lin, J., Meghraoui, M., Stein, R.S., 2008. 12 May 2008 M = 7.9 Wenchuan, China, earthquake calculated to increase failure stress and seismicity rate on three major fault systems. Geophys. Res. Lett. 35, L17305. doi:10.1029/2008GL034903.

Van der Woerd, J., et al., 2002. Uniform postglacial slip-rate along the central 600 km of the Kunlun Fault (Tibet), from 26Al, 10Be, and 14C dating of riser offsets, and climatic origin of the regional morphology. Geophys. J. Int. 148, 356–388.

Wan, Y., Shen, Z., Zeng, Y., Sheng, S., 2007. Evolution of cumulative Coulomb failure stress in northeastern Qinghai–Xizang (Tibetan) Plateau and its effect on large earthquake occurrence. Acta Seismol. Sin. 20 (2), 117–132.

Wang, C.-Y., Chan, W.W., Mooney, W.D., 2003. Three-dimensional velocity structure of crust and upper mantle in southwestern China and its tectonic implications. J. Geophys. Res. 108. doi:10.1029/2002JB001973.

Wang, W., Zhao, L., Li, J., Yao, Z., 2008a. Rupture process M_s8.0 Wenchuan earthquake of Sichuan China. Chinese J. Geophys 51 (5), 1403–1410 In Chinese.

Wang, Y., Wang, E., Shen, Z., Wang, M., Gan, W., Qiao, X., Meng, G., Li, T., Tao, W., Yang, Y., Cheng, J., Li, P., 2008b. GPS-constrained inversion of present-day slip rates along major faults of the Sichuan–Yunnan region, China. Sci China (Ser D-Earth Sci.) 51 (9), 1267–1283.

Wang, Y., Shen, Z., Wang, M. 2010. Crustal motion and deformable block model of northeastern Tibetan plateau. (submitted to Chinese J. Geophys.)

Xu, X., Wen, X., Chen, G., Yu, S., 2008. Discovery of the Longriba Fault Zone in Eastern Bayan Har Block, China and its tectonic implication. Sci China(Ser D-Earth Sci.) 51 (9), 1209–1223.

Yao, H., Beghein, C., van der Hilst, R.D., 2008. Surface wave array tomography in SE Tibet from ambient seismic noise and two-station analysis — II. Crustal and upper-mantle structure. Geophys. J. Int. 173, 205–219. doi:10.1111/j.1365-246X.2007.03696.x.

Zhang, Y., Feng, W.P., Xu, L.S., Zhou, C.H., Chen, Y.T., 2009. Spatio-temporal rupture process of the 2008 great Wenchuan earthquake. Sci. China Ser. D 52 (2), 145–154.

Zhu, A.L., Xu, X.W., Zhou, Y.S., Yin, J.Y., Gan, W.J., Chen, G.H., 2005. Relocation of small earthquakes in western Sichuan. China and its implications for active tectonics. Chinese J. Geophys. 48 (3), 692–700.